Chinese Journal of Natural Medicines

Structurally novel tryptamine–derived alkaloids from the seeds of *Peganum harmala* and their antiviral activities against respiratory syncytial virus

Zhongnan Wu, Yubo Zhang, Guocai Wang, Qing Tang, Yaolan Li, Xiaoqing Xie, Yushen Liang, Wen Cheng

Citation: Zhongnan Wu, Yubo Zhang, Guocai Wang, Qing Tang, Yaolan Li, Xiaoqing Xie, Yushen Liang, Wen Cheng, Structurally novel tryptamine–derived alkaloids from the seeds of *Peganum harmala* and their antiviral activities against respiratory syncytial virus, Chinese Journal of Natural Medicines, 2025, 23(8), 972–979. doi: 10.1016/S1875–5364(25)60932–0.

View online: https://doi.org/10.1016/S1875–5364(25)60932–0

Chinese Journal of Natural Medicines 23 (2025) 972-979

Contents lists available at ScienceDirect

Chinese Journal of Natural Medicines

journal homepage: www.cjnmcpu.com/

Original article

Structurally novel tryptamine-derived alkaloids from the seeds of *Peganum harmala* and their antiviral activities against respiratory syncytial virus

Zhongnan Wu[a,Δ*], Yubo Zhang[b,Δ], Guocai Wang[b,Δ], Qing Tang[b,Δ], Yaolan Li[b], Xiaoqing Xie[a], Yushen Liang[a], Wen Cheng[a]

[a] *The Affiliated Dongguan Songshan Lake Central Hospital, Guangdong Medical University; College of Pharmacy, Guangdong Medical University, Dongguan 523808, China*
[b] *Institute of Traditional Chinese Medicine & Natural Products, Guangdong Province Key Laboratory of Pharmacodynamic Constituents of TCM and New Drugs Research, College of Pharmacy, Jinan University, Guangzhou 510632, China*

ARTICLE INFO

Article history:
Received 23 September 2024
Revised 26 November 2024
Accepted 5 January 2025
Available online 20 August 2025

Keywords:
Peganum harmala
Tryptamine-derived alkaloid
Anti-RSV activity

ABSTRACT

Peganum harmala L. (*P. harmala*) is a significant economic and medicinal plant. The seeds of *P. harmala* have been extensively utilized in traditional Chinese medicine, Uighur medicine, and Mongolian medicine, as documented in the *Drug Standard of the Ministry of Health of China*. Twelve novel tryptamine-derived alkaloids (**1**–**12**) and eight known compounds (**13**–**20**) were isolated from *P. harmala* seeds. Compounds **1** and **2** represent the first reported instances of tryptamine-derived heteromers, comprising tryptamine and aniline fragments with previously undocumented C-3–N-1′ linkage and C-3–C-4′ connection, respectively. Compounds **3**–**5** were identified as indole-quinazoline heteromers, exhibiting a novel C-3 and NH-1′ linkage between indole and quinazoline-derived fragments. Compound **6** demonstrates the dimerization pattern of C-C linked tryptamine-quinazoline dimer. Compound **8** represents a tryptamine-derived heterodimer with a distinctive carbon skeleton, featuring an unusual spiro-tricyclic ring (**7**) and conventional bicyclic tryptamine. Compounds **9**–**11** constitute novel 6/5/5/5 spiro-tetracyclic tryptamine-derived alkaloids presenting a unique ring system of tryptamine-spiro-pyrrolizine. Compounds **1**–**3** and **6**–**11** were identified as racemates. Compounds **2**, **7**, **9**, **10**, and **12** were confirmed *via* X-ray crystallographic analysis. All isolated compounds (**1**–**20**) exhibited varying degrees of antiviral efficacy against respiratory syncytial virus (RSV). Notably, the anti-RSV activity of compound **12** (IC_{50} 5.01 ± 0.14 μmol·L^{-1}) surpassed that of the positive control (ribavirin, IC_{50} 6.23 ± 0.95 μmol·L^{-1}), as validated through plaque reduction and immunofluorescence assays. The identification of anti-RSV compounds from *P. harmala* seeds may enhance the development and application of this plant in antiviral therapeutic products.

1. Introduction

Peganum harmala L. (*P. harmala*) (Zygophyllaceae) predominantly occurs in desert areas and arid grasslands, including Xinjiang, Inner Mongolia, Ningxia, Qinghai, and Gansu Provinces of China [1-3]. This plant possesses significant economic and medicinal value. Due to its robust root system, *P. harmala* serves as an effective soil and water conservation plant. The branches and leaves of *P. harmala* contain essential micronutrients, including Fe, Mn, Cu, Zn, and various acids, making it suitable as a nutrient-rich feedstuff after frost. Furthermore, the seeds of *P. harmala* have been historically recognized as a national medicine, included in the Drug Standards, and regulated by the Ministry of Public Health of China. The plant is extensively utilized in traditional Chinese, Uighur, and Mongolian medicines for treating joint pain, rheumatoid arthritis, sciatica, *etc.* [1]. Additionally, the seeds of *P. harmala* constitute the primary active component in compound drugs such as “Compound Luotuopengzi Ointments” (http://ypk.39.net/820437/) and “Compound Muniziqi Granules” (http://ypk.39.net/822279/), which are clinically applied for joint pain treatment and endocrine regulation, respectively.

Alkaloids have been established as the primary bioactive components of this plant, exhibiting diverse biological activities, including anti-tumor [2, 4-8], anti-inflammatory [9-12], anti-viral [13-16], anti-oxidant [10, 17, 18] activities, *etc.* The present study identified twelve novel tryptamine-derived alkaloids (**1**–**12**) and eight known compounds (Fig. 1) from the crude alkaloids of *P. harmala* seeds. Compounds **1** and **2** represent unprecedented tryptamine-derived heteromers comprising tryptamine and aniline moieties connected through two distinct modes, where the moieties in **1** and **2** are linked *via* C-3–N-1′ and C-3–C-4′ interactions, respectively (Fig. 2). Compounds **3**–**5** comprise tryptamine and quinazoline fragments, featuring the previously undocumented C-3–NH-1′ linkage. Compound **7** features a distinctive 6/5/5 spirocyclic system formed by a methyl-substituted pyrrole ring connected to the tryptamine unit through a spiral atom (C-3). Com-

* Corresponding author.
E-mail address: wuzhongnan@gdmu.edu.cn (Z. Wu)
Δ These authors contributed equally to this work.

https://doi.org/10.1016/S1875-5364(25)60932-0

pound **8** represents the first reported tryptamine-derived heterodimer exhibiting an unusual 6/5/5–5/6 framework, where a rare spiro-tricyclic indole connects to a conventional bicyclic tryptamine *via* an N-12–C-3′ linkage. Compounds **8**–**11** constitute the first documented tryptamine-derived alkaloids characterized by a novel 6/5/5/5 tetracyclic spiro framework. Compounds **1**–**3** and **6**–**11** were identified as nine racemates through chiral-phase separations. The structures of compounds **2**, **7**, **9**, **10**, and **12** were confirmed by X-ray crystallography (Fig. 3).

Respiratory syncytial virus (RSV), a negative-strand RNA virus belonging to the *Paramyxoviridae* family, primarily affects human lungs, causing acute lower respiratory illness. The anti-RSV activity of isolates **1**–**20** was evaluated, demonstrating half maximal inhibitory concentration (IC_{50}) values ranging from 5.01 ± 0.14 to 51.73 ± 2.01 μmol·L^{-1}. Notably, compound **12** exhibited superior anti-RSV activity (IC_{50} 5.01 ± 0.14 μmol·L^{-1}) compared to the positive control, as determined through plaque reduction and immunofluorescence assays.

2. Results and discussion

Peganumione A (**1**) exhibited a molecular formula of $C_{25}H_{30}N_4O_6$, determined through high-resolution electrospray ionization mass spectrometry (HR-ESI-MS) analysis (ion peak at *m/z* 505.2062 [M + Na]$^+$, Calcd. for $C_{25}H_{30}N_4O_6Na$ 505.2058). The ^{1}H nuclear magnetic resonance (NMR) spectrum (Table S1) revealed two aromatic AMX spin systems [δ_H 7.78 (1H, d, *J* = 9.0 Hz), 6.18 (1H, dd, *J* = 9.0, 2.4 Hz), 5.22 (1H, d, *J* = 2.4 Hz); 7.11 (1H, d, *J* = 8.9 Hz), 6.56 (1H, dd, *J* = 8.9, 2.4 Hz), 6.56 (1H, d, *J* = 2.4 Hz)], two methoxyls [δ_H 3.75 (3H, s), 3.43 (3H, s)], two methyls [δ_H 1.79 (3H, s), 1.76 (3H, s)], and three NH protons [δ_H 9.77 (1H, br s), 7.95 (1H, t, 5.0), 7.91 (1H, t, 5.0)] in **1**. Four distinct spin systems in **1** (Fig. 2) were identified *via* ^{1}H–^{1}H correlation spectroscopy (COSY) correlations involving: H-5 (δ_H 7.11) with H-6 (δ_H 6.56); H-10 (δ_H 2.09/1.97) with H-11 (δ_H 3.05/2.98); H-4′ (δ_H 7.78) with H-5′ (δ_H 6.18); and H-9′ (δ_H 3.08) with H-10′ (δ_H 3.36). The heteronuclear multiple bond correlation (HMBC) cross-peaks from H-5 to C-3 (δ_C 62.0)/C-7 (δ_C 160.4)/C-9 (δ_C 142.3), from H-6 to C-4 (δ_C 120.7)/C-8 (δ_C 97.4), from H-8 (δ_H 6.56) to C-4/C-6 (δ_C 107.2), and from 7-OCH_3 (δ_H 3.75) to C-7 indicated a 7-methoxy tryptamine unit (**1a**, Fig. 2). Furthermore, the remaining data suggested the **1b** fragment was an aniline derivative, confirmed by the ^{1}H–^{1}H COSY correlations between H-4′ (δ_H 7.78) and H-5′ (δ_H 6.18), and between H-9′ (δ_H 3.08) and H-10′ (δ_H 3.36), along with the HMBC cross-peaks from H-4′ to C-2′ (δ_C 150.4)/C-6′ (δ_C 163.9)/C-8′ (δ_C 199.6), from H-5′ to C-3′ (δ_C 112.4)/C-7′ (δ_C 96.2), from H-7′ (δ_H 5.22) to C-3′/C-5′ (δ_C 102.9), from H-9′ to C-8′/C-10′ (δ_C 34.8), from H-10′ to C-8/C-9′ (δ_C 38.3)/C-12′ (δ_C 169.3), from H-13′ (δ_H 1.76) to C-12′, and from 6′-OCH_3 (δ_H 3.73) to C-6′. The HMBC cross-peaks from H-1′ (δ_H 9.77) to C-2 (δ_C 178.1)/C-3/C-4/C-10 (δ_C 38.7)/C-3′ (δ_C 112.4)/C-6′ (δ_C 163.9)/C-7′ (δ_C 96.2) confirmed the linkage of two fragments (**1a** and **1b**) between C-3 and N-1′. Subsequently, the enantiomer separation of **1** was performed *via* chiral high-performance liquid chromatography (HPLC) (Lux Cellulose-4 column, 250 mm × 4.6 mm, 5 μm, Phenomenex, USA, 90% MeOH/H_2O, 1.0 mL·min^{-1}, t_R 4.9 and 5.9 min), yielding (+)-**1** and (−)-**1** (Fig. S3). The electronic circular dichroism (ECD) spectrum of (+)-**1** corresponded to the calculated value of (3*R*)-**1**, while that of (−)-**1** aligned with the calculation for (3*S*)-**1** (Fig. 4).

Peganumione B (**2**), obtained as colorless needle crystals, exhibited the same molecular formula of $C_{25}H_{30}N_4O_6$ as compound **1**, as determined by HR-ESI-MS at *m/z* 505.2063 [M + Na]$^+$ (Calcd. for $C_{25}H_{30}N_4O_6Na$ 505.2058). Analysis of the 1D NMR data in Table S2 revealed the primary differences between **2** and **1**: an aromatic tertiary carbon and a –NH– group in **1** were substituted by a quaternary carbon (δ_C 117.2) and a –NH_2 group, respectively, in **2**. The C-3 chemical shift transitioned from δ_C 74.1 in **1** to δ_C 51.2 in **2**, suggesting that two fragments (**2a** and **2b**) were connected through a C-C bridge between C-3 and C-4′ in **2**. This structural feature was confirmed *via* the HMBC cross-peaks from H-10 (δ_H 2.18) to C-5′ (δ_C 117.2) and from H-4′ (δ_H 7.78)/H-7′ (δ_H 6.17) to

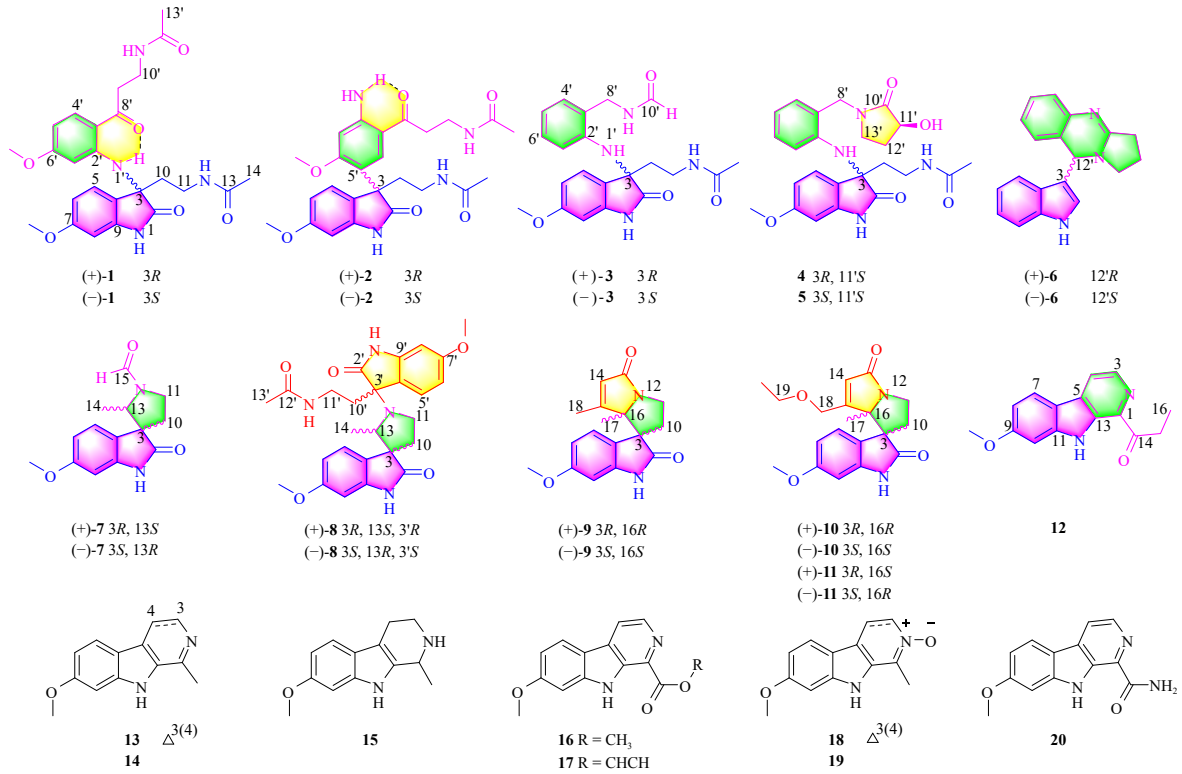

Fig. 1 Chemical structures of **1**–**20**.

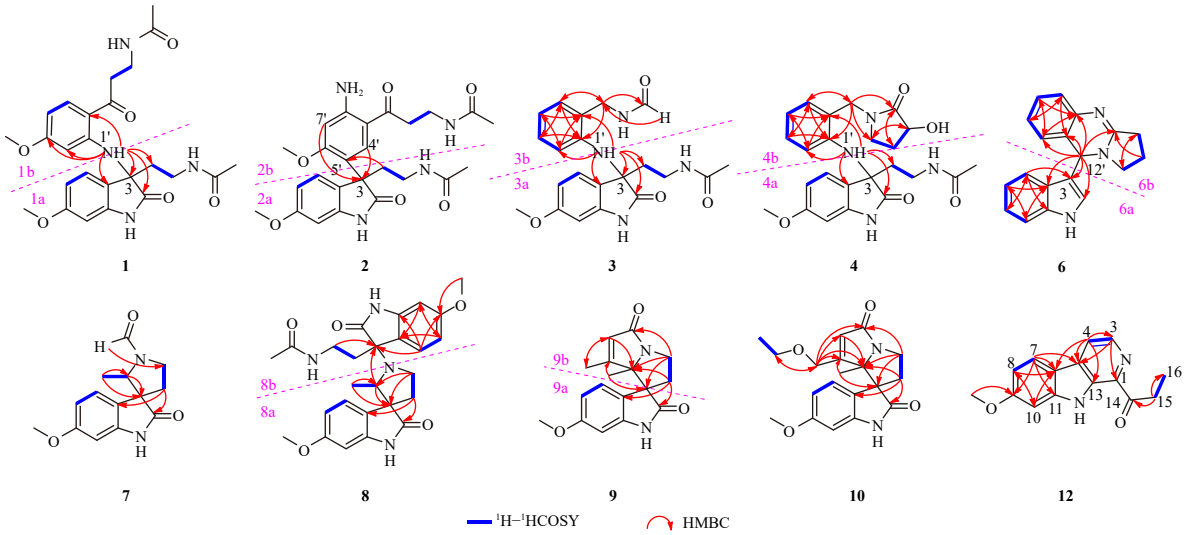

Fig. 2 Key ^{1}H–^{1}H COSY and HMBC correlations of **1**–**4**, **6**–**10**, and **12**.

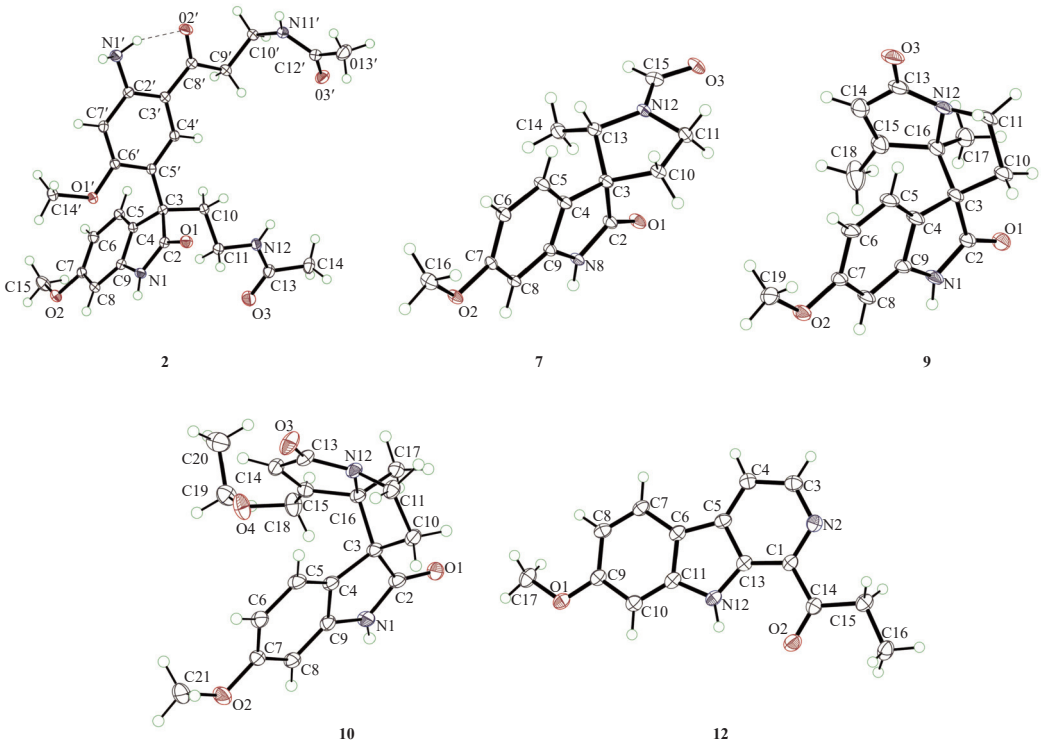

Fig. 3 An X-ray ORTEP diagram of **2**, **7**, **9**, **10**, and **12**.

C-3 (δ_C 51.2) (Fig. 2). The structure of compound **2** was further verified through X-ray diffraction analysis (Fig. 3). Additionally, compound **2**, possessing a stereogenic center, displayed an optical rotation of $[\alpha]_D^{25}$ +0.1 (*c* 1.0, MeOH), indicating its racemic nature. Subsequently, enantiomeric resolution of **2** was performed *via* chiral HPLC, yielding a pair of enantiomers (±)-**2** (Fig. S4). The calculated and measured ECD spectra of (3*R*)-**2** and (3*S*)-**2** corresponded to (+)-**2** and (−)-**2**, respectively (Fig. 4).

Peganumione C (**3**), with the molecular formula $C_{21}H_{24}N_4O_4$, was isolated as a whitish powder. The ^{1}H–^{1}H COSY correlations (Table S3) between H-5 (δ_H 7.01) and H-6 (δ_H 6.50), between H-10 (δ_H 2.07/2.00) and H-11 (δ_H 2.96/2.85), between H-4′ (δ_H 7.02) and H-5′ (δ_H 6.49), between H-5′ and H-6′ (δ_H 6.77), and between H-6′ and H-7′ (δ_H 5.68) demonstrated the presence of five spin systems in **3** (Fig. 2). The HMBC cross-peaks from H-5 to C-3 (δ_C 62.6)/C-7 (δ_C 160.0)/C-9 (δ_C 142.3), from H-6 to C-4 (δ_C 121.4)/C-8 (δ_C 97.1), from H-8 (δ_H 6.48) to C-4/C-6 (δ_C 106.9), and from 7-OCH$_3$ (δ_H 3.74) to C-7 indicated the presence of a 7-methoxyindole moiety (**3a**, Fig. 2). Additional evidence revealed a 1,2-disubstituted benzene ring connected to a –CH$_2$NHCHO group and a –NH– moiety (**3b**, Fig. 2), which was confirmed by the HMBC cross-peaks from H-4′ to C-2′ (δ_C 143.6)/C-6′ (δ_C 128.1)/C-8′ (δ_C 38.0), from H-5′ to C-3′ (δ_C 123.8)/C-7′ (δ_C 111.4), H-6′ to C-2′/C-4′ (δ_C 130.0), from H-7′ to C-3′/C-5′ (δ_C 116.9), from H-8′ (δ_H 4.30) to C-2′/C-4′/C-10′ (δ_C 161.8), and from H-10′ (δ_H 8.17) to C-8′ (δ_C 38.0). The aforementioned fragments (**3a** and **3b**) were connected *via* the C-N bond (C-3–NH-1′), as confirmed by the HMBC cross-peaks from NH-1′ (δ_H 5.87) to C-2 (δ_C 179.0)/C-3/C-4/C-10 (δ_C 38.9)/C-3′/C-7′ (Fig. 2). Subsequently, enantiomeric compounds, (+)-**3** and (−)-**3**, achieved chirality through chiral

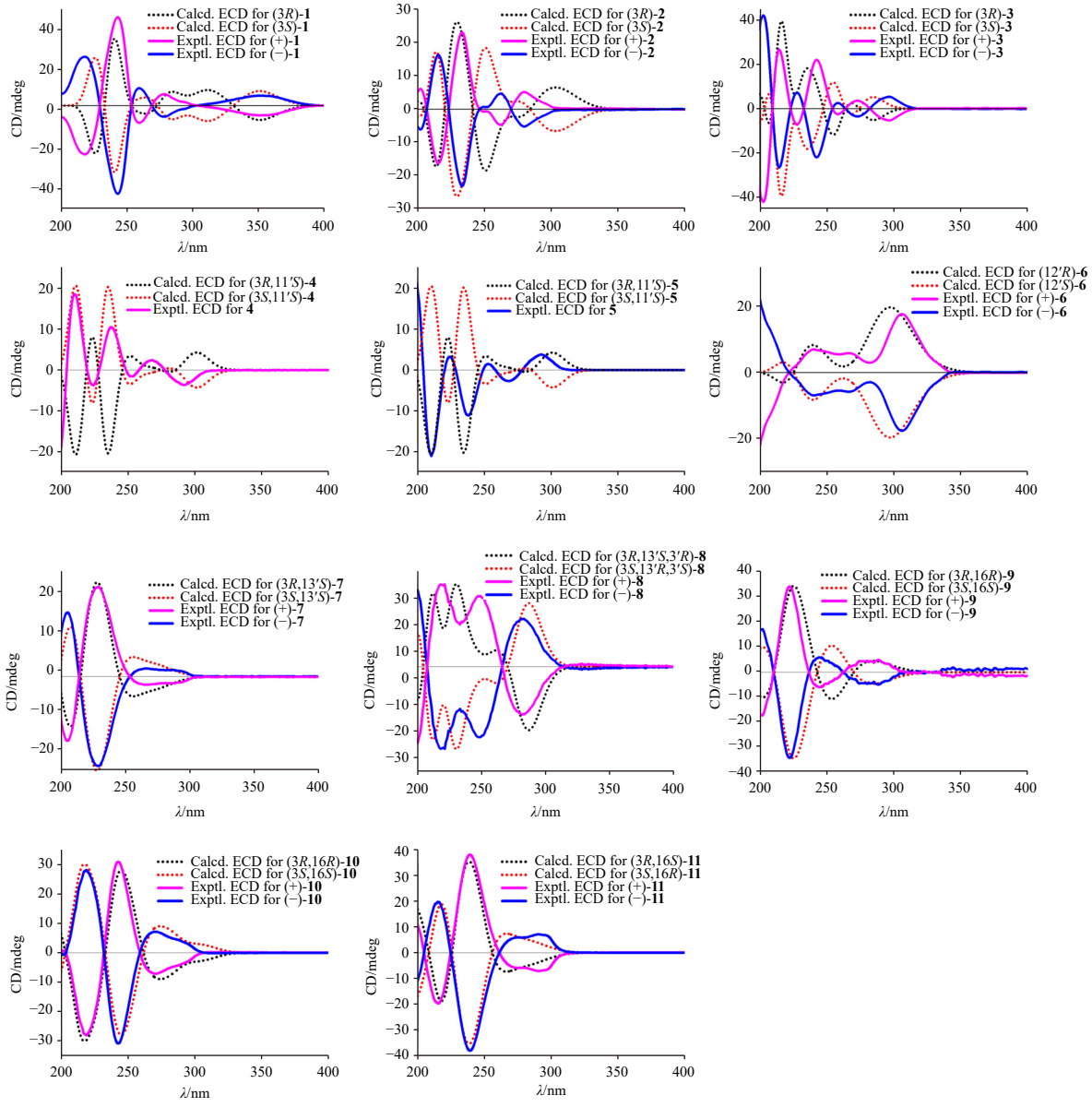

Fig. 4 Calculated and experimental ECD spectra of (±)-**1**–**3**, **4**, **5**, and (±)-**6**–**11**, respectively.

HPLC separation (Fig. S5). The computed ECD spectra of both (3*R*)-**3** and (+)-**3** showed weak compliance with experimental results, while those of (3*S*)-**3** and (−)-**3** demonstrated accurate correlation (Fig. 4).

Peganumione D (**4**) was isolated as a white solid with an $[\alpha]_D^{25}$ +36.2 (*c* 1.0, CH_2Cl_2). The molecular formula, $C_{24}H_{28}N_4O_5$, was determined through ^{13}C NMR and HR-ESI-MS analysis (*m/z* 475.1958 $[M + Na]^+$, Calcd. for $C_{24}H_{28}N_4O_5Na$ 475.1952). The 1D NMR data (Table S4) of **4** exhibited minor differences compared to those of **3**, primarily in the absence of the −NHCHO group in **3** and the presence of the butyrolactam ring in **4** (Fig. 1). These observations suggested that the −NHCHO group was substituted by the butyrolactam ring in **4**, which was confirmed through analysis of the ^1H–^1H COSY correlations of H-11′ (δ_H 4.26)/H-12′ (δ_H 2.29/2.07) and H-12′/H-13′ (δ_H 3.25/3.08), along with the HMBC cross-peaks from H-8′ (δ_H 4.42/4.30) to C-10′ (δ_C 174.7)/C-13′ (δ_C 42.7), from H-11′ to C-13′, from H-12′ to C-10′, and from H-13′ to C-11′ (δ_C 69.0) (Fig. 2). The absolute configuration of the secondary alcohol at C-11′ was determined using a transition metal chelate dirhodium reagent $Rh_2(OCOCF_3)_4$ [19-21]. Based on the bulkiness rule [21], the *E* band (350 nm) of the induced ECD spectra of the *in situ* complexes of the chiral alcohol with $Rh_2(OCOCF_3)_4$ showed positive values (Fig. S1), confirming the absolute configuration of C-11′ as *S*. Furthermore, the absolute stereochemistry of **4** was verified through quantum-mechanical ECD analysis. The calculated ECD spectra of (3*R*,11′*S*)-**4** and (3*S*,11′*S*)-**4** were generated using TDDFT-ECD methodology. The experimental ECD spectrum of **4** matched the theoretical (3*R*,11′*S*)-**4** spectrum (Fig. 4), establishing the absolute stereochemistry of **4** as 3*R*,11′*S*.

Peganumione E (**5**) had the molecular formula $C_{24}H_{28}N_4O_5$ determined by HR-ESI-MS (*m/z* 475.1956 $[M + Na]^+$, Calcd. for $C_{24}H_{28}N_4O_5Na$ 475.1952). The NMR spectra of compound **5** (Table S5) closely resembled those of **4**, indicating a similar planar structure. Notably, compounds **5** and **4** displayed identical NMR profiles while exhibiting different HPLC retention times. The rotation values of **5** (+19.1) and **4** (+36.2) were both positive, suggesting they were not enantiomers. The stereochemistry of C-11′ *S* in **5** was confirmed *via* the induced ECD of the *in situ* formed $Rh_2(OCOCF_3)_4$ complex (Fig. S1), matching that of **4**. These findings indicated that **5** and **4** were epimers with opposite absolute configurations at C-3. Comparison with the theoretical ECD spectra of **5**, (3*R*,11′*S*)-**5** and (3*S*,11′*S*)-**5** (Fig. 4) confirmed the absolute stereochemistry of **5** as 3*S*,11′*S*.

Peganumione F (**6**) was determined to be $C_{19}H_{17}N_3$ through HR-ESI-MS analysis (*m/z* 288.1494 [M + H]$^+$, Calcd. for $C_{19}H_{18}N_3$, 288.1495). Analysis of 1D and 2D data (Table S6) revealed the **6a** fragment (Fig. 1) as a tryptamine unit, confirmed by ^{1}H–^{1}H COSY correlations of H-5 (δ_H 7.28)/H-6 (δ_H 6.87), H-6/H-7 (δ_H 7.03), and H-7/H-8 (δ_H 7.34), along with the HMBC cross-peaks from H-5 to C-3 (δ_C 117.0)/C-7 (δ_C 121.2)/C-9 (δ_C 136.9), from H-6 to C-4 (δ_C 124.9)/C-8 (δ_C 111.7), from H-7 to C-5 (δ_C 118.9)/C-9, and from H-8 to C-4/C-6 (δ_C 118.9) (Fig. 2). The remaining data indicated the **6b** fragment (Fig. 1) resembled deoxyvasicinone [7], except for the replacement of the carbonyl group with a methine at C-12′ [δ_H 5.99 (1H, s); δ_C 53.4] in **6b**. The fragments **6a** and **6b** were connected through a C-C bond between C-3 and C-12′, confirmed by HMBC cross-peaks from H-12′ (δ_H 5.99) to C-2 (δ_C 123.6)/C-3/C-4/C-4′ (δ_C 161.3)/C-6′ (δ_C 143.2)/C-10′ (δ_C 127.1)/C-11′ (δ_C 123.7) (Fig. 2). The enantiomeric pair (+)-**6** and (−)-**6** was separated *via* chiral HPLC (Fig. S6), identified as (12′*R*)-**6** and (12′*S*)-**6** respectively through comparison of their measured and predicted ECD curves (Fig. 4).

Peganumione G (**7**) appeared as colorless crystals with a molecular formula of $C_{14}H_{16}N_2O_3$ determined by HR-ESI-MS analysis (*m/z* 283.1053 [M + Na]$^+$, Calcd. for $C_{14}H_{16}N_2O_3Na$ 283.1053). The ^{1}H–^{1}H COSY correlations (Table S7) of H-5 (δ_H 7.17)/H-6 (δ_H 6.54), of H-10 (δ_H 2.19/2.13)/H-11 (δ_H 3.64), and of H-13 (δ_H 3.99)/H-14 (δ_H 1.08) indicated three spin systems in **7** (Fig. 2). The HMBC cross-peaks (Fig. 2) from H-5 to C-3 (δ_C 55.8)/C-7 (δ_C 159.9)/C-9 (δ_C 143.5), from H-6 to C-4 (δ_C 121.1)/C-8 (δ_C 96.4), from H-8 (δ_H 6.42) to C-4/C-6 (δ_C 106.7), and from 7-OCH$_3$ (δ_H 3.73) to C-7 established a 7-methoxy tryptamine unit. The remaining spectral data revealed a pyrrole ring connected to the 7-methoxy tryptamine unit *via* a spiral atom (C-3), forming a novel spiro-tricyclic system. This structure was confirmed by HMBC cross-peaks from H-10 to C-2 (δ_C 178.6)/C-3 and from H-14 to C-3/C-13 (δ_C 59.7). Additionally, HMBC cross-peaks from H-15 (δ_H 8.20) to C-11 (δ_C 42.7)/C-13 demonstrated the aldehyde group's linkage to the pyrrole ring's N atom. The nuclear Overhauser effect spectroscopy (NOESY) spectrum (Fig. S2) showed a NOE correlation between H-13 (δ_H 3.99) and H-10, indicating that these protons are spatially close and located on the same face of the molecule. The structure of **7** was further confirmed through single-crystal X-ray diffraction (Fig. 3). The enantiomers, (+)-**7** and (−)-**7**, were separated *via* chiral HPLC (Fig. S7). The predicted ECD spectra of (3*R*,13*S*)-**7** and (3*S*,13*R*)-**7** showed remarkable similarity to those observed in (+)-**7** and (−)-**7**, respectively (Fig. 4).

Peganumione H (**8**) was characterized by its molecular formula of $C_{26}H_{30}N_4O_5$ through HR-ESI-MS analysis (*m/z* 479.2289 [M + H]$^+$, Calcd. for $C_{26}H_{31}N_4O_5$ 479.2289). NMR analysis (Table S8) revealed that the **8a** fragment exhibited similarity to compound **7**, with the distinction that the aldehyde group was reduced in the **8a** fragment. This structural feature was confirmed by the ^{1}H–^{1}H COSY correlations between H-5 (δ_H 7.28) and H-6 (δ_H 6.51), between H-10 (δ_H 2.08/1.83) and H-11 (δ_H 3.63/3.20), and between H-13 (δ_H 3.19) and H-14 (δ_H 0.76), along with the HMBC cross-peaks from H-5 to C-3 (δ_C 56.1)/C-7 (δ_C 159.3)/C-9 (δ_C 142.3), from H-6 to C-4 (δ_C 127.0)/C-8 (δ_C 95.9), from H-8 (δ_H 6.35) to C-4/C-6 (δ_C 106.4), from 7-OCH$_3$ (δ_H 3.71) to C-7, from H-10 to C-2 (δ_C 179.6)/C-3/C-4, from H-11 to C-3/C-10 (δ_C 34.0)/C-13 (δ_C 62.8), from H-13 to C-2/C-3/C-4/C-10, and from H-14 to C-3/C-13 (Fig. 2). Additionally, the remaining spectral data indicated that the **8b** fragment demonstrated similarity to the tryptamine alkaloid peganumaline B [7], with the notable difference that the chemical shift of C-3′ changed from δ_C 74.1 in peganumaline B to δ_C 66.3 in **8b**, suggesting the replacement of the oxygenated quaternary carbon (C-3′) in peganumaline B with a quaternary carbon connected to the N atom in **8b**. The spectral evidence indicated that the two fragments (**8a** and **8b**) were connected through the C–N bond between N-12 and C-3′, as confirmed by the HMBC cross-peaks from H-13 to C-3′ (δ_C 66.3) (Fig. 2). The relative stereochemistry of **8** was established through analysis of the NOESY spectrum (Fig. S2). The NOE correlations between H-13 and H-10 and between H-14 and H-10′ (δ_H 3.76/3.70) established the relative configuration of **8** as 3R^*,13S^*,3′R^*. Subsequently, chiral HPLC separated the pair of enantiomers (+)-**8** and (−)-**8** (Fig. S8), revealing the structures of (3*R*,13*S*,3′*R*)-**8** and (3*S*,13*R*,3′*S*)-**8**, which were confirmed through ECD spectroscopy (Fig. 4).

Peganumione I (**9**)'s molecular formula, $C_{17}H_{18}N_2O_3$, was established through its HR-ESI-MS data (*m/z* 321.1224 [M + Na]$^+$, Calcd. for $C_{17}H_{18}N_2O_3Na$ 321.1210). The ^{1}H–^{1}H COSY (Table S9) correlations of H-5 (δ_H 6.40)/H-6 (δ_H 6.42), and of H-10 (δ_H 2.90/2.20)/H-11 (δ_H 3.64/3.43) indicated two spin systems in **9** (Fig. 2). The HMBC cross-peaks from H-5 to C-3 (δ_C 54.1)/C-7 (δ_C 159.4)/C-9 (δ_C 142.0), from H-6 to C-4 (δ_C 122.4)/C-8 (δ_C 96.5), from H-8 (δ_H 6.43) to C-4/C-6 (δ_C 106.4), and from 7-OCH$_3$ (δ_H 3.69) to C-7 established a 7-methoxy tryptamine unit (**9a**, Fig. 1). Further analysis revealed a *tri*-substituted pyrrolizine ring with two methyl groups (**9b**, Fig. 1), confirmed through HMBC cross-peaks from H-10 to C-11 (δ_C 40.1)/C-16 (δ_C 77.2), from H-11 to C-10 (δ_C 38.5)/C-13 (δ_C 173.2)/C-16, from H-14 (δ_H 5.50) to C-13/C-15 (δ_C 163.4)/C-16/C-18 (δ_C 12.7), from H-17 (δ_H 1.45) to C-15/C-16, and from H-18 (1.42) to C-13/C-14 (δ_C 122.4)/C-15/C-16 (Fig. 2). The aforementioned fragments (**9a** and **9b**) were connected through a spiral atom (C-3) to form a novel spiro-tetracyclic system, as evidenced by HMBC cross-peaks from H-10 to C-2 (δ_C 177.0)/C-3/C-4, from H-11 to C-3, and from H-17 to C-3 (Fig. 2). Compound **9** was ultimately characterized as a rare spirocyclic alkaloid with a 6/5/5/5 ring system through single-crystal X-ray diffraction (Cu Kα) (Fig. 3). Subsequently, enantiomers (+)-**9** and (−)-**9** were separated using chiral HPLC (Fig. S9). The predicted ECD spectrum of (3*R*,16*R*)-**9** corresponded to that of (+)-**9** (Fig. 4), while the simulated curve of (3*S*,16*S*)-**9** aligned with that measured for (−)-**9**.

Peganumione J (**10**), colorless crystals, exhibited a molecular formula of $C_{19}H_{22}N_2O_4$, determined by HR-ESI-MS analysis (*m/z* 343.1660 [M + H]$^+$, Calcd. for $C_{19}H_{23}N_2O_4$ 343.1652). The NMR spectroscopic data (Table S10) of compound **10** shared similarities with **9**, featuring the same 6/5/5/5 tetracyclic spiro ring skeleton. The primary distinctions included the absence of a methyl (C-18) and the presence of oxygenated methylenes and an additional ethoxyl group in **10**. The ethoxyl moiety's bond to C-18 was confirmed through the ^{1}H–^{1}H COSY correlation of H-19 (δ_H 3.03/2.99)/H-20 (δ_H 0.94), and key HMBC correlations from H-18 (3.96/3.50) to C-13 (δ_C 172.4)/C-14 (δ_C 121.2)/C-15 (δ_C 164.1)/C-16 (δ_C 76.0)/C-19 (δ_C 65.6), from H-19 to C-18 (δ_C 65.0)/C-20 (δ_C 14.8), and from H-20 to C-19 (Fig. 2). Compound **10** was subsequently confirmed as an unusual spirocyclic alkaloid with a unique 6/5/5/5 imidazolidine framework through single-crystal X-ray diffraction Cu Kα analysis (Fig. 3). The enantiomers, (+)-**10** and (−)-**10**, were separated through chiral HPLC (Fig. S10). The computed ECD spectrum of (3*R*,16*R*)-**10** demonstrated excellent correlation with the experimental data of (+)-**10** (Fig. 4), while the calculated value of (3*S*,16*S*)-**10** precisely matched the measured data of (−)-**10**.

Peganumione K (**11**) was determined to have a molecular formula of $C_{19}H_{22}N_2O_4$ through HR-ESI-MS analysis (*m/z* 343.1653 [M + H]$^+$, Calcd. for $C_{19}H_{23}N_2O_4$ 343.1652). The 1D NMR data (Table S11) of **11** aligned with that of **10**, sharing a 6/5/5/5 tetracyclic spiro framework, with notable differences in chemical shifts of C-2, C-4, C-5, C-10, C-15, C-16, C-17 from δ_C 176.8, 122.6, 124.3, 39.0, 164.1, 76.0, 20.4 in **10** to δ_C 178.2, 118.8, 126.3, 37.2, 161.1, 74.2, 21.6 in **11**, respectively. These variations indicated different configurations at C-3 or C-16 in **11** compared to **10**. The NOESY spectrum (Fig. S2) revealed a correlation between H-10

(δ_H 2.90/2.33)/H-17 (δ_H 1.45), indicating the relative stereochemistry of **11** as 3R^*,16S^*. Compounds **11** (3R^*,16S^*) and **10** (3R^*,16R^*) were thus identified as epimers. The enantiomeric pairs (+)-**11** and (−)-**11** were isolated *via* chiral HPLC (Fig. S11) and established as (3*R*,16*S*)-**11** and (3*S*,16*R*)-**11** based on ECD calculations (Fig. 4).

HR-ESI-MS analysis of peganumione L (PL) (**12**) (*m/z* 255.1126 [M + H]$^+$, Calcd. for $C_{15}H_{15}N_2O_2$ 255.1128) indicated a molecular formula of $C_{15}H_{14}N_2O_2$. Comparative analysis of spectral data between compound **12** (Table S12) and harmine [22] indicated that they shared an identical tricyclic *β*-carboline skeleton. The primary distinction between **12** and harmine was the replacement of a methyl group with a propanoyl group [δ_C 204.2 (C=O), 30.8 (CH_2), 8.4 (CH_3); δ_H 3.33 (2H, q, *J* = 7.3 Hz), 1.19 (3H, t, *J* = 7.3 Hz)] in **12**, indicating that the methyl group (connecting to C-1) in harmine was substituted by a propanoyl group in **12** (Fig. 1). The structure was confirmed *via* the ^{1}H–^{1}H COSY correlation of H_2-15 (δ_H 3.33)/H_3-16 (δ_H 1.19), along with the HMBC correlations from H_2-15 to C-14 (δ_C 204.2)/C-16 (δ_C 8.4), and from H_3-16 to C-14/C-15 (δ_C 30.8) (Fig. 2). Furthermore, compound **12** was verified *via* X-ray diffraction analysis (Fig. 3).

Based on the reported spectroscopic data, the eight known alkaloids were characterized as harmine (**13**) [22], harmaline (**14**) [22], tetrahydroharmine (**15**) [23], harmic acid methyl ester (**16**) [8], harmic acid ethyl ester (**17**) [8], harmine *N*-oxide (**18**) [8], pegaharmine I (**19**) [8], and harmic amide (**20**) [8].

2.1. Antiviral activities against RSV of compounds 1–20

Previous research demonstrated that *β*-carboline alkaloids from *P. harmala* exhibited significant anti-HSV-2 virus effects [16], while the anti-RSV activities of other indole alkaloids remain largely unexplored. Consequently, the isolates (**1**–**20**) were evaluated for RSV antivirulence through plaque reduction and CPE assays. Compounds **1**–**20** exhibited potent RSV inhibitory effects with IC_{50} values ranging from 5.01 ± 0.14 to 51.73 ± 2.01 μmol·L^{-1} (Table 1). Notably, PL (**12**) exhibited the most potent anti-RSV activity (IC_{50} 5.01 ± 0.14 μmol·L^{-1}), subsequently confirmed by immunofluorescence assay. Methyl thiazolyl tetrazolium (MTT) analysis revealed PL's cytotoxicity (Fig. 5A) on HEp-2 cells, with CC_{50} values of 75.81 ± 1.75 μmol·L^{-1}. PL's tolerance to high titer virus infection was assessed by infecting HEp-2 cells with RSV at varying titers (MOI = 0.1, 1, or 5) (Fig. 5B). At non-toxic concentrations, PL's plaque inhibition of RSV was evaluated through plaque reduction assay (Fig. 5C). Results demonstrated that simultaneous application of PL and RSV to HEp-2 cells significantly reduced virus production in a concentration-dependent manner. The virus yield assay (Fig. 5D) revealed maximum progeny virus generation by third post-RSV infection. PL (40 μmol·L^{-1}) significantly suppressed RSV proliferation during the initial four days. These findings confirmed that PL's significant antiviral effect against RSV was independent of cytotoxicity. Green fluorescence indicated elevated levels of viral F proteins within this virus population. PL treatment substantially reduced RSV-induced green fluorescence (Fig. 5E). The data demonstrate PL's robust anti-RSV activity across various infectious levels.

3. Conclusion

In summary, twelve novel tryptamine-derived alkaloids (**1**–**12**, peganumiones A–M) and eight known compounds were isolated from *P. harmala* seeds. Structural elucidation was accomplished through comprehensive spectroscopic analysis (IR, UV, HR-ESI-MS, and 1D and 2D NMR), complemented by X-ray crystallography, ECD calculations and the $Rh_2(OCOCF_3)_4$-induced ECD spectrum. All compounds exhibited varying levels of anti-RSV activity. Notably, PL (**12**) demonstrated the most potent antiviral effect against RSV with an IC_{50} value of 5.01 ± 0.14 μmol·L^{-1}. Significantly, PL's anti-RSV activity surpasses that of ribavirin, the positive control. This research identifies novel antiviral alkaloids from *P. harmala* seeds, providing valuable guidance for developing active anti-RSV components from this plant.

Table 1 *In vitro* anti-RSV activity of compounds **1**–**20** (mean ± SD, *n* = 3).

Compounds	RSV		
	IC_{50}/(μmol·L^{-1})[a]	CC_{50}/(μmol·L^{-1})[b]	SI[c]
(+)-**1**	35.18 ± 1.12	> 100	> 2.8
(−)-**1**	31.21 ± 1.01	> 100	> 3.2
(+)-**2**	44.56 ± 1.22	> 100	> 2.2
(−)-**2**	39.27 ± 1.06	> 100	> 2.5
(+)-**3**	46.22 ± 1.32	> 100	> 2.2
(−)-**3**	51.73 ± 2.01	> 100	> 1.9
4	39.71 ± 1.95	> 100	> 2.5
5	35.62 ± 1.66	> 100	> 2.8
(+)-**6**	22.39 ± 0.31	89.12 ± 4.11	4.0
(−)-**6**	23.71 ± 0.42	92.33 ± 4.55	3.9
(+)-**7**	23.81 ± 1.01	91.46 ± 4.32	3.8
(−)-**7**	31.16 ± 1.76	> 100	> 3.2
(+)-**8**	38.12 ± 1.28	> 100	> 2.6
(−)-**8**	35.28 ± 1.17	> 100	> 2.8
(+)-**9**	22.13 ± 0.52	96.22 ± 5.32	4.3
(−)-**9**	19.22 ± 0.42	82.25 ± 4.61	4.3
(+)-**10**	23.01 ± 0.64	97.55 ± 4.91	4.2
(−)-**10**	28.43 ± 0.85	93.83 ± 5.56	3.3
(+)-**11**	41.59 ± 1.57	> 100	> 2.4
(−)-**11**	37.11 ± 1.23	> 100	> 2.7
12	5.01 ± 0.14	75.81 ± 1.75	15.1
13	18.43 ± 0.25	79.96 ± 5.35	4.4
14	21.17 ± 0.33	90.91 ± 7.02	4.3
15	25.61 ± 0.22	96.22 ± 6.55	3.8
16	11.29 ± 0.64	98.17 ± 6.82	8.7
17	12.71 ± 1.02	> 100	> 7.9
18	29.79 ± 1.01	> 100	> 3.4
19	22.16 ± 0.76	96.71 ± 7.27	4.4
20	9.61 ± 0.44	78.58 ± 5.26	8.2
Ribavirin[d]	6.23 ± 0.95	> 100	> 16.1

[a]IC_{50} is the concentration of compound that reduced 50% CPE as compared with control cells infected with the virus; [b]CC_{50} is the concentration of compound with half maximal inhibition on the growth and survival of host cells; [c]Selectivity index (SI) = CC_{50}/IC_{50}; [d]Positive control.

4. Experimental

4.1. General experimental procedures

Details of the experimental equipment can be found in Supporting information.

4.1.1. Plant material

Details of the plant material can be found in Supporting information.

4.1.2. Extraction and isolation

P. harmala seeds (12 kg) were pulverized and extracted with a 95% CH_3CH_2OH/H_2O mixture (30 L × 3) at room temperature. The extract concentrate (956 g) was dissolved in 4 L of water, and the solution's pH was adjusted to 3 using 5% HCl. The acidic extract underwent fractionation with CH_2Cl_2 (4 L × 3), producing a CH_2Cl_2-soluble fraction. The acid layer's pH was adjusted to 9 using a 30% ammonium hydroxide solution. The alkali phase was then partitioned with CH_2Cl_2 (4 L × 3), yielding an alkaloid extract (315 g). The raw alkaloids underwent D101 macroporous

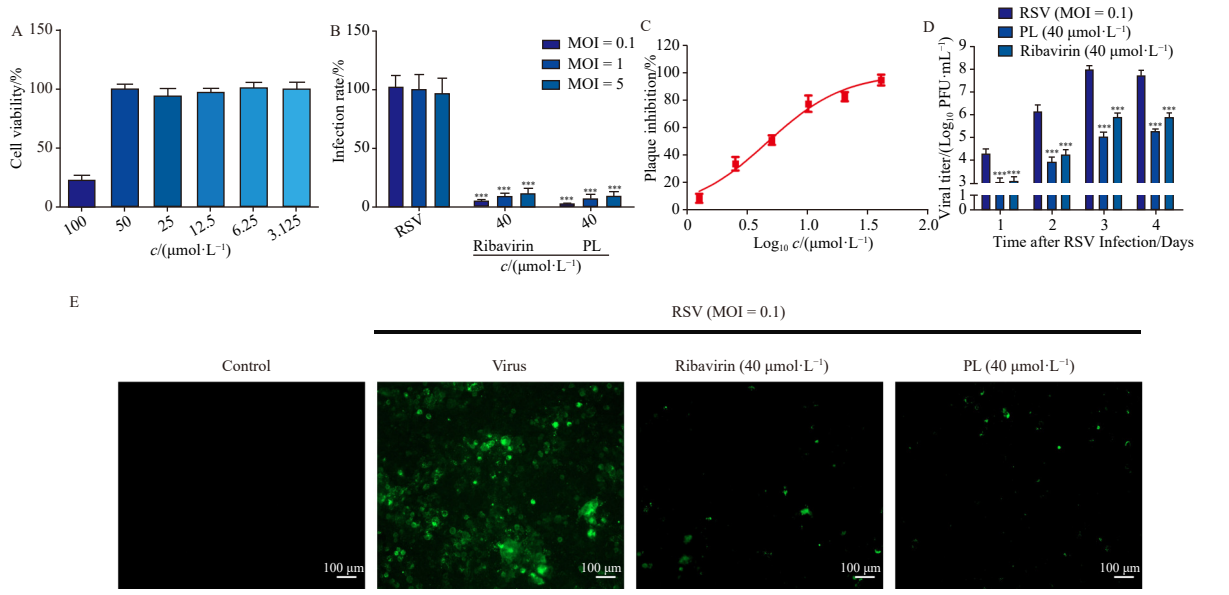

Fig. 5 Antiviral activity (RSV) and cytotoxicity of PL (**12**) *in vitro*. (A, C) The monolayer (HEp-2 cells) was treated with PL (100, 50, 25, 12.5, 6.25, or 3.125 μmol·L^{-1}) or a mixture of PL (40, 20, 10, 5, 2.5, or 1.25 μmol·L^{-1}) and virus (RSV, MOI = 0.1). Cell viability and viral titers were tested by MTT and plaque reduction assay, respectively. (B) The monolayer (HEp-2 cells) was inoculated with a mixture consisting of PL (40 μmol·L^{-1}) and an equal volume of virus (RSV, MOI = 0.1, 1, or 5). Ribavirin (40 μmol·L^{-1}) was used as positive control. After 48 h incubation, supernatants were collected from each well and viral titers were tested by plaque assay. (D) The monolayer (HEp-2 cells) was inoculated with a mixture consisting of PL (40 μmol·L^{-1}) and an equal volume of virus (RSV, MOI = 0.1). Ribavirin (40 μmol·L^{-1}) was used as positive control. Supernatants were collected from each well at the indicated time after virus infection. Viral titers were tested by plaque assay. (E) The monolayer (HEp-2 cells) was inoculated with a mixture consisting of PL (40 μmol·L^{-1}) and an equal volume of virus (RSV, MOI = 0.1). Ribavirin (40 μmol·L^{-1}) was used as positive control. After 24 h of incubation, HEp-2 cells were stained with anti-RSV F antibodies, and fluorescence intensity in HEp-2 cells was determined by fluorescence microscopy. Data are presented as mean ± SD of three independent experiments. $^{***}P < 0.001$ *vs* the viral control group).

adsorption resin chromatography using ethanol/water gradient (10∶90, 30∶70, 50∶50, 70∶30, 95∶5, *V*/*V*), producing five fractions (Frs. A–E). Fr. C (22.3 g), subjected to silica gel chromatography using a CH_2Cl_2/MeOH gradient (10∶90 to 100∶0, *V*/*V*), yielded seven derivative fractions (Frs. C1–C7). Fr. C5 (1.8 g) was chromatographed through Sephadex LH-20 (CH_2CI_2/MeOH, 2∶1, *V*/*V*), yielding compounds **1** (16.2 mg), **2** (17.1 mg), and **3** (22.5 mg). Fr. C4 (3.8 g) underwent ODS CC using a MeOH/H_2O gradient (10∶90 to 100∶0, *V*/*V*), yielding **4** (15.2 mg), **5** (9.7 mg), and **6** (10.9 mg). Fr. C3 (1.8 g) was refined using Sephadex LH-20 (CH_2Cl_2/MeOH, 2∶1, *V*/*V*), followed by preparative HPLC (MeOH/H_2O/NH_4OH, 70∶30∶0.01, *V*/*V*/*V*), yielding **7** (9.9 mg), **8** (6.8 mg), and **9** (13.7 mg). Fr. C2 (2.5 g) underwent purification *via* preparative HPLC using a MeOH/H_2O/NH_4OH ratio of 60∶40∶0.01 *V*/*V*/*V*, yielding compounds **10** (11.9 mg), **11** (15.5 mg), and **12** (22.1 mg).

Peganumione A (**1**): white amorphous powder; mp: 181–182 °C; (+)-**1**: $[\alpha]_D^{25}$ +37.2 (*c* 1.0, CH_2Cl_2); (−)-**1**: $[\alpha]_D^{25}$ −36.5 (*c* 1.0, CH_2Cl_2); UV (CH_2Cl_2) λ_{max} (log ε): 217 (1.71), 269 (0.23) nm; IR (KBr) ν_{max} 3387, 1666, 1604, 1483, 1468, 1382, 1337, 1320, 1296, 1273, 1223, 1169, 1149, 1107, 1057, 994, 894, 779, 702 cm^{-1}; for NMR spectroscopic data (Table S1); HR-ESI-MS *m*/*z* 505.2062 [M + Na]$^+$ (Calcd. for $C_{25}H_{30}N_4O_6Na$, 505.2058).

Peganumione B (**2**): colorless needle crystals (CH_3OH/H_2O); mp: 169–170 °C; (+)-**2**: $[\alpha]_D^{25}$ +26.8 (*c* 1.0, CH_2Cl_2); (−)-**2**: $[\alpha]_D^{25}$ −27.5 (*c* 1.0, CH_2Cl_2); UV (CH_2Cl_2) λ_{max} (log ε): 223 (2.56), 265 (0.61), 295 (0.58) nm; IR (KBr) ν_{max} 3420, 3219, 1648, 1569, 1542, 1385, 1270, 1157, 1143, 1033, 832, 791, 716 cm^{-1}; for NMR spectroscopic data (Table S2); HR-ESI-MS *m*/*z* 505.2063 [M + Na]$^+$ (Calcd. for $C_{25}H_{30}N_4O_6Na$, 505.2058).

Crystal data of **2**: $C_{25}H_{30}N_4O_6$, *Mr* = 482.53, triclinic, *a* = 10.7973 (4) Å, *b* = 11.1314 (4) Å, *c* = 12.1954 (5) Å, α = 116.275 (4)°, β = 105.219 (4)°, γ = 100.367 (3)°, *V* = 1191.61 (9) Å^3, *T* = 149.99 (10), *Z* = 2, μ(Cu Kα) = 0.803 mm^{-1}, reflections collected 8064 which were used in all calculations. Final *R* indexes [all data] R_1 = 0.0520, wR_2 = 0.1264, and the goodness of fit on F^2 was equal to 1.058. CCDC number: 2048242 (http://www.ccdc.cam.ac.uk/).

Peganumione C (**3**): white amorphous powder; (+)-**3**: $[\alpha]_D^{25}$ +31.2 (*c* 1.0, CH_2Cl_2); (−)-**3**: $[\alpha]_D^{25}$ −32.7 (*c* 1.0, CH_2Cl_2); UV (CH_2Cl_2) λ_{max} (log ε): 217 (0.48), 278 (0.07) nm; IR (KBr) ν_{max} 3142, 3071, 1624, 1565, 1480, 1450, 1414, 1384, 1328, 1290, 1275, 1237, 1198, 1162, 1101, 1027, 941, 810, 757 cm^{-1}; for NMR spectroscopic data (Table S3); HR-ESI-MS *m*/*z* 419.1687 [M + Na]$^+$ (Calcd. for $C_{21}H_{24}N_4O_4Na$ 419.1690).

Peganumione D (**4**): white amorphous powder; $[\alpha]_D^{25}$ +36.2 (*c* 1.0, CH_2Cl_2); UV (CH_2Cl_2) λ_{max} (log ε): 210 (0.28), 265 (0.15), 318 (0.11) nm; IR (KBr) ν_{max} 3397, 1660, 1613, 1483, 1467, 1379, 1343, 1320, 1290, 1275, 1225, 1172, 1133, 1104, 991, 775 cm^{-1}; for NMR spectroscopic data (Table S4); HR-ESI-MS *m*/*z* 475.1958 [M + Na]$^+$ (Calcd. for $C_{24}H_{28}N_4O_5Na$ 475.1952).

Peganumione E (**5**): white amorphous powder; $[\alpha]_D^{25}$ +19.1 (*c* 1.0, CH_2Cl_2); UV (CH_2Cl_2) λ_{max} (log ε): 207 (0.26), 265 (0.16), 317 (0.10) nm; IR (KBr) ν_{max} 3397, 1660, 1613, 1482, 1379, 1343, 1320, 1290, 1275, 1225, 1172, 1104, 991, 775, 701 cm^{-1}; for NMR spectroscopic data (Table S5); HR-ESI-MS *m*/*z* 475.1956 [M + Na]$^+$ (Calcd. for $C_{24}H_{28}N_4O_5Na$ 475.1952).

Peganumione F (**6**): white amorphous powder; (+)-**6**: $[\alpha]_D^{25}$ +33.7 (*c* 1.0, CH_2Cl_2); (−)-**6**: $[\alpha]_D^{25}$ −31.2 (*c* 1.0, CH_2Cl_2); UV (CH_2Cl_2) λ_{max} (log ε): 205 (1.32), 234 (0.61), 287 (0.25) nm; IR (KBr) ν_{max} 3405, 3328, 3178, 3047, 1683, 1616, 1467, 885, 775 cm^{-1}; For NMR spectroscopic data (Table S6); HR-ESI-MS *m*/*z* 288.1494 [M + H]$^+$ (Calcd. for $C_{19}H_{18}N_3$ 288.1495).

Peganumione G (**7**): colorless needle crystals (CH_3OH/H_2O); mp 173–174 °C; (+)-**7**: $[\alpha]_D^{25}$ +19.7 (*c* 1.0, CH_2Cl_2); (−)-**7**: $[\alpha]_D^{25}$ −18.9 (*c* 1.0, CH_2Cl_2); UV (CH_2Cl_2) λ_{max} (log ε): 199 (0.12), 225 (0.22), 266 (0.06), 306 (0.04) nm; IR (KBr) ν_{max} 3382, 3174, 1681, 1660, 1625, 1611, 1466, 1387, 1320, 1281, 1117, 1102, 773 cm^{-1}; for NMR spectroscopic data (Table S7); HR-ESI-MS *m*/*z* 283.1053 [M + Na]$^+$ (Calcd. for $C_{14}H_{16}N_2O_3Na$ 283.1053).

Crystal data of **7**: $C_{14}H_{16}N_2O_3$, *Mr* = 260.29, triclinic, *a* = 7.4680 (5) Å, *b* = 7.9039 (4) Å, *c* = 11.2215 (5) Å, α = 105.661 (4)°, β = 96.294 (5)°, γ = 95.078 (5)°, *V* = 629.08 (6) Å^3, *T* = 150.00 (10) K, *Z* = 2, μ(Cu Kα) = 0.803 mm^{-1}, reflections collected 4058 which were used in all calculations. Final *R* indexes [all

data] R_1 = 0.0701, wR_2 = 0.1841, and the goodness of fit on F^2 was equal to 1.041. CCDC number: 2104687 (http://www.ccdc.cam.ac.uk/).

Peganumione H (**8**): white amorphous powder; (+)-**8**: $[\alpha]_D^{25}$ +41.5 (*c* 1.0, CH_2Cl_2); (−)-**8**: $[\alpha]_D^{25}$ −42.0 (*c* 1.0, CH_2Cl_2); UV (CH_2Cl_2) λ_{max} (log ε): 200 (0.12), 225 (0.21), 266 (0.07), 309 (0.03) nm; IR (KBr) ν_{max} 3431, 3387, 1683, 1660, 1627, 1607, 1464, 1381, 1325, 1278, 1124, 1109, 769 cm^{-1}; for NMR spectroscopic data (Table S8); HR-ESI-MS *m/z* 479.2289 $[M + H]^+$ (Calcd. for $C_{26}H_{31}N_4O_5$ 479.2289).

Peganumione I (**9**): colorless needle crystals (CH_3OH/H_2O); mp 173–174 °C; (+)-**9**: $[\alpha]_D^{25}$ +22.3 (*c* 1.0, CH_2Cl_2); (−)-**9**: $[\alpha]_D^{25}$ −23.1 (*c* 1.0, CH_2Cl_2); UV (CH_2Cl_2) λ_{max} (log ε): 223 (2.50), 265 (0.62), 295 (0.60) nm; IR (KBr) ν_{max} 3298, 2949, 2843, 1698, 1627, 1556, 1509, 1464, 1347, 1275, 1189, 1159, 1133, 1021 cm^{-1}; For NMR spectroscopic data (Table S9); HR-ESI-MS *m/z* 321.1224 $[M + Na]^+$ (Calcd. for $C_{17}H_{18}N_2O_3Na$ 321.1210).

Crystal data of **9**: $C_{17}H_{18}N_2O_3{\cdot}(H_2O)_{0.5}$, *Mr* = 307.34, monoclinic, *a* = 13.047 (3) Å, *b* = 8.8417 (10) Å, *c* = 14.030 (3) Å, α = 90°, β = 112.43(2)°, γ = 90°, *V* = 1496.0 (5) $Å^3$, *T* = 149.99 (10) K, *Z* = 4, μ(Cu Kα) = 0.789 mm^{-1}, reflections collected 5561 which were used in all calculations. Final *R* indexes [all data] R_1 = 0.1188, wR_2 = 0.2534, and the goodness of fit on F^2 was equal to 1.091. CCDC number: 2105283 (http://www.ccdc.cam.ac.uk/).

Peganumione J (**10**): colorless needle crystals (CH_3OH/H_2O); mp 162–163 °C; (+)-**10**: $[\alpha]_D^{25}$ +19.8 (*c* 1.0, CH_2Cl_2); (−)-**10**: $[\alpha]_D^{25}$ −18.9 (*c* 1.0, CH_2Cl_2); UV (CH_2Cl_2) λ_{max} (log ε): 209 (0.41), 283 (0.08) nm; IR (KBr) ν_{max} 3353, 1684, 1500, 1456, 1306, 1255, 1204, 1137, 755 cm^{-1}; for NMR spectroscopic data (Table S10); HR-ESI-MS *m/z* 343.1660 $[M + H]^+$ (Calcd. for $C_{19}H_{23}N_2O_4$ 343.1652).

Crystal data of **10**: $C_{19}H_{22}N_2O_4$, *Mr* = 342.38, orthorhombic, *a* = 15.8543 (5) Å, *b* = 16.9397 (5) Å, *c* = 25.7318 (8) Å, α = 90°, β = 90°, γ = 90°, *V* = 6910.7 (4) $Å^3$, *T* = 100.0 (3) K, *Z* = 16, μ(Cu Kα) = 0.760 mm^{-1}, reflections collected 34437 which were used in all calculations. Final *R* indexes [all data] R_1 = 0.0589, wR_2 = 0.1548, and the goodness of fit on F^2 was equal to 1.034. CCDC number: 2049205 (http://www.ccdc.cam.ac.uk/).

Peganumione K (**11**): white amorphous powder; (+)-**11**: $[\alpha]_D^{25}$ +21.4 (*c* 1.0, CH_2Cl_2); (−)-**11**: $[\alpha]_D^{25}$ −22.3 (*c* 1.0, CH_2Cl_2); UV (CH_2Cl_2) λ_{max} (log ε): 211 (0.43), 272 (0.06) nm; IR (KBr) ν_{max} 3340, 3267, 1669, 1495, 1456, 1385, 1101, 758 cm^{-1}; for NMR spectroscopic data (Table S11); HR-ESI-MS *m/z* 343.1653 $[M + H]^+$ (Calcd. for $C_{19}H_{23}N_2O_4$ 343.1652).

Peganumione L (**12**): colorless needle crystals (CH_3OH/H_2O); mp 178–179 °C; $[\alpha]_D^{25}$ +9.8 (*c* 1.0, CH_2Cl_2); UV (CH_2Cl_2) λ_{max} (log ε): 223 (1.38), 298 (0.26) nm; IR (KBr) ν_{max} 3441, 2926, 1625, 1542, 1453, 1370, 1276, 1201, 1159, 1131, 1074, 1027, 979, 946, 902, 826 cm^{-1}; for NMR spectroscopic data (Table S12); HR-ESI-MS *m/z* 255.1126 $[M + H]^+$ (Calcd. for $C_{15}H_{15}N_2O_2$ 255.1128).

Crystal data of **12**: $C_{15}H_{14}N_2O_2$, *Mr* = 254.28, monoclinic, *a* = 28.963 (6) Å, *b* = 4.9129 (8) Å, *c* = 35.584 (8) Å, α = 90°, β = 101.34 (2)°, γ = 90°, *V* = 4964.4 (18) $Å^3$, *T* = 150.00 (10) K, *Z* = 16, μ(Cu Kα) = 0.745 mm^{-1}, reflections collected 20122 which were used in all calculations. Final *R* indexes [all data] R_1 = 0.1534, wR_2 = 0.2662, and the goodness of fit on F^2 was equal to 1.010. CCDC number: 2334094 (http://www.ccdc.cam.ac.uk/).

4.1.3. Antiviral activity assay in vitro

The anti-RSV activity of all compounds was evaluated using an MTT assay, a plaque reduction assay, and the CPE test. Detailed experimental procedures are available in Supporting information.

Funding

This work was supported by the National Natural Science Foundation of China (Nos. 82104015, 82003609, 81973190), the Guangdong Basic and Applied Basic Research Foundation (Nos. 2020A1515110415, 2020A1515110453, 2020B1515020033), the Characteristic Innovation Project of General Universities in Guangdong Province (No. 2024KTSCX167) and the Science and Technology Planning Project of Guangzhou City (No. 202201010485).

Supporting information

Supporting information for this work is available from the corresponding authors *via* E-mail.

Declaration of competing interest

These authors have no conflict of interest to declare.

References

1 Ma J, Wang XL. The species and distribution of genus *Peganum* L. in the desert area of China. *J Desert Res*. 1998;18(2):131-136.
2 Li SG, Zhang Q, Wang YT, et al. *β*-Carboline alkaloids from the roots of *Peganum harmala* L. *Chin J Nat Med*. 2024;22(2):171-177. https://doi.org/10.1016/S1875-5364(24)60583-2.
3 Anstis DG, Liyu J, Davison EK, et al. Alkaloids from the entheogenic plant *Peganum harmala*. *Aust J Chem*. 2023;76:264-278. https://doi.org/10.1071/CH23038.
4 Zhang Q, Zan YH, Yang HG, et al. Anti-tumor alkaloids from *Peganum harmala*. *Phytochemistry*. 2022;197:113107. https://doi.org/10.1016/j.phytochem.2022.113107.
5 Xu Y, Zhao X, Zhang D, et al. New *β*-carboline alkaloids from the seeds of *Peganum harmala*. *Phytochem Lett*. 2023;53:166-169. https://doi.org/10.1016/j.phytol.2022.12.015.
6 Li SG, Wang KB, Gong C, et al. Cytotoxic quinazoline alkaloids from the seeds of *Peganum harmala*. *Bioorg Med Chem Lett*. 2018;28(2):103-106. https://doi.org/10.1016/j.bmcl.2017.12.003.
7 Wang KB, Hu X, Li SG, et al. Racemic indole alkaloids from the seeds of *Peganum harmala*. *Fitoterapia*. 2018;125:155-160. https://doi.org/10.1016/j.fitote.2018.01.008.
8 Wang KB, Li DH, Bao Y, et al. Structurally diverse alkaloids from the seeds of *Peganum harmala*. *J Nat Prod*. 2017;80(2):551-559. https://doi.org/10.1021/acs.jnatprod.6b01146.
9 Liu JB, Li WY, Zhao X, et al. Peganutonin A, a novel melatonin analogue from the seeds of *Peganum harmala*. *Phytochem Lett*. 2023;56:78-80. https://doi.org/10.1016/j.phytol.2023.07.002.
10 Abbas MW, Hussain M, Qamar M, et al. Antioxidant and anti-inflammatory effects of *Peganum harmala* extracts: an *in vitro* and *in vivo* study. *Molecules*. 2021;26(19):6084. https://doi.org/10.3390/molecules26196084.
11 Liu X, Li MX, Tan S, et al. Harmine is an inflammatory inhibitor through the suppression of NF-*κ*B signaling. *Biochem Biophys Res Commun*. 2017;489(3):332-338. https://doi.org/10.1016/j.bbrc.2017.05.126.
12 Niu XF, Yao Q, Li WF, et al. Harmine mitigates LPS-induced acute kidney injury through inhibition of the TLR4-NF-*κ*B/NLRP3 inflammasome signalling pathway in mice. *Eur J Pharmacol*. 2019;849:160-169. https://doi.org/10.1016/j.ejphar.2019.01.062.
13 Zhu ZH, Zhao SJ, Wang CH. Antibacterial, antifungal, antiviral, and antiparasitic activities of *Peganum harmala* and its ingredients: a review. *Molecules*. 2022;27(13):4161. https://doi.org/10.3390/molecules27134161.
14 Benzekri R, Bouslama L, Papetti A, et al. Anti HSV-2 activity of *Peganum harmala* (L.) and isolation of the active compound. *Microb Pathog*. 2018;114:291-298. https://doi.org/10.1016/j.micpath.2017.12.017.
15 Chen DY, Su AR, Fu YX, et al. Harmine blocks herpes simplex virus infection through downregulating cellular NF-*κ*B and MAPK pathways induced by oxidative stress. *Antiviral Res*. 2015;123:27-38. https://doi.org/10.1016/j.antiviral.2015.09.003.
16 Wu ZN, Chen NH, Tang Q, et al. *β*-Carboline alkaloids from the seeds of *Peganum harmala* and their anti-HSV-2 virus activities. *Org Lett*. 2020;22(18):7310-7314. https://doi.org/10.1021/acs.orglett.0c02650.
17 Herraiz T, Guilln H, Arn VJ, et al. Identification, occurrence and activity of quinazoline alkaloids in *Peganum harmala*. *Food Chem Toxicol*. 2017;103:261-269. https://doi.org/10.1016/j.fct.2017.03.010.
18 Herraiz T, Guilln H. Monoamine oxidase: a inhibition and associated antioxidant activity in plant extracts with potential antidepressant actions. *Biomed Res Int*. 2018;2018:4810394. https://doi.org/10.1155/2018/4810394.
19 Frelek J, Szczepek WJ. $[Rh_2(O_2CCF_3)_4]$ as an auxiliary chromophore in chiroptical studies on steroidal alcohols. *Tetrahedron Asymmetr*. 1999;10:1507-1520. https://doi.org/10.1016/S0957-4166(99)00115-9.
20 Gerards M, Snatzke G. Circular dichroism, XCIII determination of the absolute configuration of alcohols, olefins, epoxides, and ethers from the CD of their "*in situ*" complexes with $[Rh_2(O_2CCF_3)_4]$. *Tetrahedron Asymmetr*. 1990;1:221-236. https://doi.org/10.1016/S0957-4166(00)86328-4.
21 Xia GY, Wang M, Chen LX, et al. Application of dirhodium reagent $Rh_2(O_2CCF_3)_4$ to the determination of the absolute configurations of secondary and tertiary alcohols. *J Int Pharm Res*. 2015;42:726-733. https://doi.org/10.13220/j.cnki.jipr.2015.06.006.
22 Talat Z, Ali Y, Aisa HA. Isolation of alkaloids from "*Kursi caper*" by countercurrent chromatography with pH-dependent distribution. *Chem Nat Compd*. 2014;50:968-969. https://doi.org/10.1007/s10600-014-1136-0.
23 Stefan V, Verena R, Carina D, et al. Sequence-based *in-silico* discovery, characterisation, and biocatalytic application of a set of imine reductases. *ChemCatChem*. 2018;10(15):3236-3246. https://doi.org/10.1002/cctc.201800607.